Vector diffraction analysis by discrete-dipole approximation

Kei Shimura

Mechanical Systems Laboratory, Corporate Research & Development Center, Toshiba Corporation, 1, Komukai Toshiba-cho, Saiwai-ku, Kawasaki 212-8582, Japan

Tom D. Milster

Optical Data Storage Center/Optical Sciences Center, University of Arizona, Tucson, Arizona 85721

Received December 29, 2000; revised manuscript received April 3, 2001; accepted April 4, 2001

The discrete-dipole approximation is applied to vector diffraction analysis in a system with large-numerical-aperture (NA) optics and subwavelength targets. Distributions of light diffracted by subwavelength dielectric targets are calculated in a solid angle that corresponds to a NA of 0.9, and their dependence on incident polarization, target shape, and target size is studied. Electric field distributions inside the target are also shown. Basic features of the vector diffraction are clearly demonstrated. This technique facilitates understanding of the vectorial effects in systems that are expected to be applied in the future to optical data storage.

OCIS codes: 050.1940, 260.1960, 290.0290.

1. INTRODUCTION

Diffraction analysis based on vectorial methods has become increasingly important for development of optical data storage systems. The dimensions of marks on recording media are already comparable with or smaller than the wavelength of light, and the dimensions are decreasing as recording density increases. In addition, the numerical aperture (NA) of the optical system is increasing beyond 0.6 because optical systems with large NAs are required for reproducing signals from such small structures.

The discrete-dipole approximation (DDA) method[1,2] is one of the powerful analysis methods based on vectorial techniques. This method was developed for scattering analysis in the field of astrophysics. Comparison with other methods such as the finite-difference time-domain method, the volume integral equation method, and the extended boundary condition method shows the advantage of the DDA in terms of flexibility in the modeling of the scatterers and computation time in scattering analysis.[3] Since this method was originally developed for scattering analysis in which many inhomogeneous scatterers are oriented randomly in space, the DDA has been used only to calculate orientational averages of scattered-light distribution, which is the main focus of interest in the field. However, the DDA can be applied to the analysis of distributions of light diffracted by subwavelength structures. In addition, flexibility in modeling the scatterers in the DDA can be of great advantage in diffraction analysis.

We apply the DDA to the analysis of two-dimensional distributions of light diffracted by structures on the scale that is of interest with respect to optical data storage.[4] We calculate distributions of light diffracted by a dielectric target in vacuum. We also calculate the electric field distributions inside the target as an aid in understanding the vectorial behavior of the light. The dependence of the distributions on incident polarization, target shape, and target size is studied. The vectorial effects in the system with large-NA optics and subwavelength targets are clearly demonstrated.

2. DISCRETE-DIPOLE APPROXIMATION

The DDA method was originally developed for analysis of scattering of light by interstellar dust grains, which are modeled as arbitrarily-shaped inhomogeneous particles. In this method the inhomogeneous particles are represented by a three-dimensional array of point dipoles. The spacing between the dipoles is smaller than the wavelength of the incident light but apparently is larger than the space between molecules or atoms in the particles. Each dipole at position $\mathbf{r}_j$ has an oscillating polarization P_j in response to both incident light $E_{\mathrm{inc},j}$ and the electric fields that are due to the other dipoles in the array:

$$P_j = \alpha_j \left(E_{\mathrm{inc},j} - \sum_{k \neq j} A_{jk} P_k \right), \tag{1}$$

where α_j is the polarizability at $\mathbf{r}_j$, $E_{\mathrm{inc},j}$ is the electric field at $\mathbf{r}_j$ that is due to the incident plane wave:

$$E_{\mathrm{inc},j} = E_0 \exp(i\mathbf{k} \cdot \mathbf{r}_j - i\omega t), \tag{2}$$

and $-A_{jk}P_k$ is the electric field at $\mathbf{r}_j$ that is due to dipole P_k at location $\mathbf{r}_k$.

Each element A_{jk} is a 3×3 matrix:

$$A_{jk} = \frac{1}{4\pi\epsilon_0}\frac{\exp(ikr_{jk})}{r_{jk}}\left[k^2(\hat{r}_{jk}\hat{r}_{jk} - 1_3) + \frac{ikr_{jk} - 1}{{r_{jk}}^2}(3\hat{r}_{jk}\hat{r}_{jk} - 1_3)\right] \quad (j \neq k), \quad (3)$$

where ϵ_0 is the dielectric constant of vacuum, $k \equiv \omega/c$, $r_{jk} \equiv |\mathbf{r}_j - \mathbf{r}_k|$, $\hat{r}_{jk} \equiv (\mathbf{r}_j - \mathbf{r}_k)/r_{jk}$, and 1_3 is the 3×3 identity matrix.

The method of assigning dipole polarizability is the key issue in the DDA. The simplest method is that of Clausius–Mosotti polarizability:

$$\alpha_j^{\mathrm{CM}} = 3d^3\epsilon_0\frac{\epsilon_j - \epsilon_0}{\epsilon_j + 2\epsilon_0}, \quad (4)$$

where ϵ_j is the dielectric constant at position $\mathbf{r}_j$ and d is the spacing between the dipoles. However, this method is exact only for the limit $kd \to 0$. Several methods for assigning polarizability are proposed to improve the approximation. The lattice dispersion relation (LDR) prescription[5] is one of those methods and yields reasonable results when $|n|kd < 1$, where n is the complex refractive index. The error in scattering efficiency factors for a dielectric sphere ($|n| \sim 2$) is within a few percent. In the LDR prescription, polarizability is written as

$$\alpha_j^{\mathrm{LDR}} = \frac{\alpha_j^{\mathrm{CM}}}{1 + (\alpha_j^{\mathrm{CM}}/d^3)[(b_1 + {n_j}^2 b_2 + {n_j}^2 b_3 S)(kd)^2 - (2/3)i(kd)^3]}, \qquad S = \sum_{j=1}^{3}(\hat{a}_j\hat{e}_j^{\,2}), \quad (5)$$

where $b_1 = -1.891531$, $b_2 = 0.1648469$, $b_3 = -1.7700004$, n_j is the complex refractive index, and $\hat{a}_j$ and $\hat{e}_j$ are unit vectors that define the incident direction and the polarization state, respectively.

Defining $A_{jj} \equiv {\alpha_j}^{-1}$, we formulate the scattering problem described with Eq. (1) as a set of inhomogeneous linear complex vector equations:

$$\sum_{k=1}^{N} A_{jk}P_k = E_{\mathrm{inc},j}, \quad (6)$$

where N is the total number of dipoles.

The self-consistent solution for the dipole polarizations can be obtained by solution of this set of equations. We use the complex-conjugate gradient method to solve the equation. In the field of astrophysics the dipole polarizations P_k are used to calculate extinction and absorption cross sections for the scattering analysis.

Computation resources required for the DDA have been studied by Draine and Flatau.[2] According to their estimation, the memory requirement is approximately $0.6N/1000$ MBytes, and the typical computation time is $0.03N$–$0.3N$ CPU s with a Sun 4/50 (Sparkstation IPX) workstation.

3. VECTOR DIFFRACTION ANALYSIS

We apply the DDA to the analysis of two-dimensional distributions of light diffracted by arbitrarily shaped subwavelength structures. This method is suitable for calculating diffraction from complex structures because target structures are described as an array of point dipoles on a lattice. Any structures—spherical, cubic, periodic, nonperiodic, multilayered, lamellar, inhomogeneous, and so on—can be handled easily in the same way. The memory requirements may limit the applicability of this method for large targets with fine structures in them. However, analysis of small targets is sufficient for many cases, including optical data storage systems, in which incident light is focused onto a small area on a recording medium. In addition, all the boundary conditions are automatically satisfied in the DDA, because interaction of the electric field in the target volume is fully considered in solution of the problem as in the volume integral equation method.

The DDA code[6] developed by Draine and Flatau is modified for our purpose and is used in our calculations. The lattice dispersion relation is used as a prescription for the dipole polarizability.

A. System Configuration and Parameters Used in the Calculations

The configuration of the optics assumed in our calculation is shown in Fig. 1. A dielectric particle in vacuum is assumed as the target structure. We selected this simple target as an aid to understanding the basic features of vector diffraction. Much more complicated targets such as multiple particles in vacuum, particles buried in dielectric materials, and particles in multilayered structures can be dealt with by this method. Wavelength λ of the incident light is 650 nm. Incident light E_{inc} is a plane wave that is linearly polarized in the xz plane (Fig. 1). Incident angle θ_i is 0 or 64°. The light scattered backward is collected by the ideal collection optics with a NA of 0.9. The second incident angle (64°) corresponds to the marginal ray angle for the collection optics. This angle and this NA of the collection optics are selected because an objective lens with a NA of ~0.9 is expected to be applied in the next-generation optical data storage systems. The irradiance distribution of the diffracted light at the pupil of the collection optics is studied.

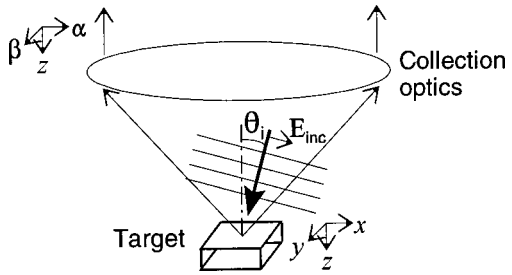

Fig. 1. Layout of the target and the collection optics assumed in the calculations.

A dielectric disk and a dielectric square plate are used as targets. The refractive index of the dielectric material is 2.15, and the thickness of the target is $\lambda/50$ (13 nm). We select two diameters for the disk, $\lambda/2$ (325 nm) and λ (650 nm), and two sizes for the square plate, $\lambda/2 \times \lambda/2$ (325 nm $\times$ 325 nm) and $\lambda \times \lambda$ (650 nm $\times$ 650 nm) with which to examine the effect of the size and the shape of the target. We use a three-dimensional matrix with 160,000 elements ($200 \times 200 \times 4$) to describe each target.

The sampling distance at the target or the spacing between the dipoles, d, is $\lambda/197$ (3.3 nm). This small sampling distance is selected so the thin (13-nm-thick) target is described satisfactorily. The DDA with the LDR prescription generally requires that $|n|kd < 1$ [$d < \lambda/(2\pi|n|)$, $d < 48$ nm in this case] for valid calculations. Accurate calculation results can be expected because d is sufficiently small ($|n|kd \simeq 0.07$).

Dipole polarizations P are calculated by complex-conjugate gradient iteration until a specified level of accuracy is achieved. The results shown in this paper converge until

$$e_{\text{local}} \equiv \frac{|A \times P - E_{\text{inc}}|}{|E_{\text{inc}}|} \leqslant 5 \times 10^{-5}, \tag{7}$$

except for some results presented in Section 4 below.

A personal computer with a Pentium III 500-MHz processor and 256-MByte memory was used, and the typical computation time for a distribution of diffracted light was 25 min or less.

B. Distributions of Diffracted Light

When dipole polarizations P_j are obtained, the diffracted field in far-field region is calculated:

$$E_{\text{far}}(\mathbf{r}) = \frac{1}{4\pi\epsilon_0} \frac{k^2 \exp(ikr)}{r} \sum_{j=1}^{N} \exp(-ik\hat{r} \cdot \mathbf{r}_j) \times (\hat{r}\hat{r} - 1_3)P_j, \tag{8}$$

where $r \equiv |\mathbf{r} - \mathbf{r}_j|$ and $\hat{r} \equiv (\mathbf{r} - \mathbf{r}_j)/r$.

We studied the dependence of the diffraction pattern on target size and shape and on incident polarization by comparing patterns for targets with different sizes and shapes.

Calculation results for normal incidence are shown in Figs. 2–4. The targets that correspond to these distributions are dielectric disks with diameters of $\lambda/2$ (325 nm) and λ (650 nm) and a dielectric square plate of sides $\lambda/2 \times \lambda/2$ (325 nm $\times$ 325 nm), respectively. Figures 2–4 show the irradiance distributions of the diffracted light at the pupil of the collection optics. In each of these figures, both the two-dimensional distribution at the pupil and profiles of the α and β axes are shown. Coordinates α and β are normalized by the focal length of the collection optics. The direction of the incident polarization at the target is parallel to the x direction in Fig. 1, which corresponds to the horizontal direction (α direction) in the distribution [Figs. 2–4(a)].

The distributions in Figs. 2 and 4 show strong polarization dependence. The profiles in the α and the β directions [Figs. 2(b) and 4(b)] are largely different from each other. Although, in comparison to the wavelength of the light, the size of the disk is not sufficiently small to be negligible, the distributions look similar to the distribution of the radiation from a point dipole located at the center of the disk and oscillating in the x direction. In addition, these two distributions are similar in spite of the difference in the target shape. The distribution in Fig. 3, however, shows weak polarization dependence. The profiles in Fig. 3(b) show that the distribution is almost rotationally symmetric, although the incident light is linearly polarized. These results show that the size of the target has a greater influence on the diffraction pattern than does the shape of the target in this case.

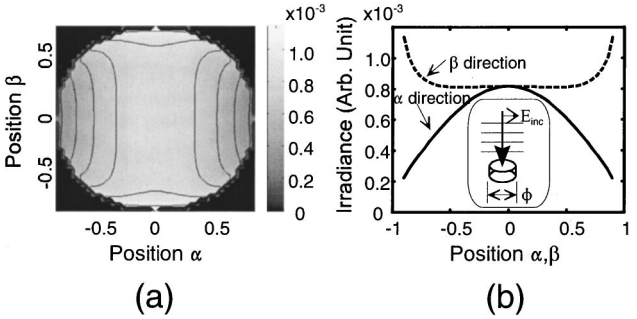

Fig. 2. Distribution of light diffracted by a small dielectric disk: (a) irradiance distribution, (b) cross section of (a). The diameter and the thickness of the disk are $\lambda/2$ and $\lambda/50$, respectively. The refractive index of the disk is 2.15. The incident light is linearly polarized, and the incident angle is 0°.

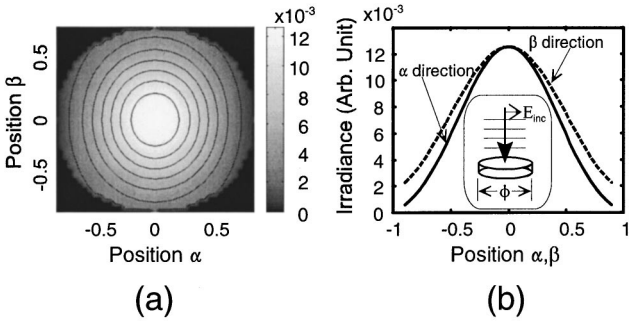

Fig. 3. Distribution of light diffracted by a large dielectric disk: (a) irradiance distribution, (b) cross section of (a). The diameter and the thickness of the disk are λ and $\lambda/50$, respectively. The refractive index of the disk is 2.15. The incident light is linearly polarized, and the incident angle is 0°.

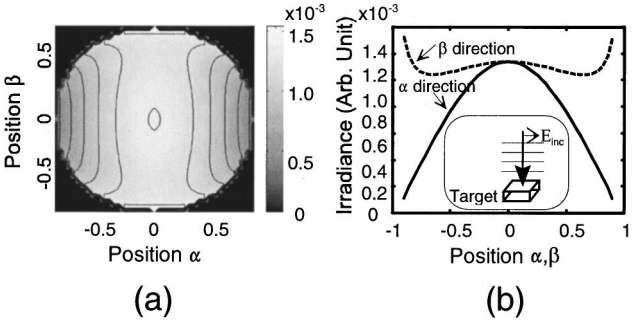

Fig. 4. Distribution of light diffracted by a small dielectric square plate: (a) irradiance distribution, (b) cross section of (a). The length of a side and the thickness of the square are $\lambda/2 \times \lambda/2$ and $\lambda/50$, respectively. The refractive index of the plate is 2.15. The incident light is linearly polarized, and the incident angle is 0°.

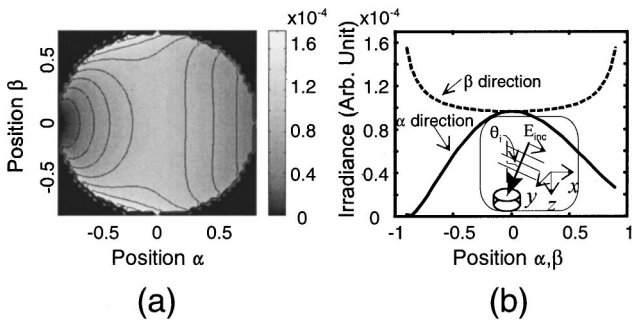

Fig. 5. Distribution of light diffracted by a small dielectric disk: (a) irradiance distribution, (b) cross section of (a). The diameter and the thickness of the disk are λ/2 and λ/50, respectively. The refractive index of the disk is 2.15. The incident light is linearly polarized, and the incident angle is 64° (p polarization).

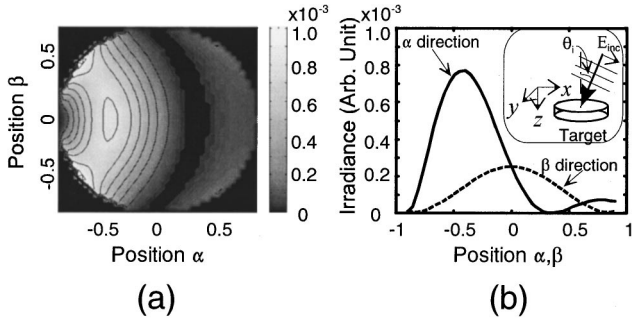

Fig. 6. Distribution of light diffracted by a large dielectric disk: (a) irradiance distribution, (b) cross section of (a). The diameter and the thickness of the disk are λ and λ/50, respectively. The refractive index of the disk is 2.15. The incident light is linearly polarized, and the incident angle is 64° (p polarization).

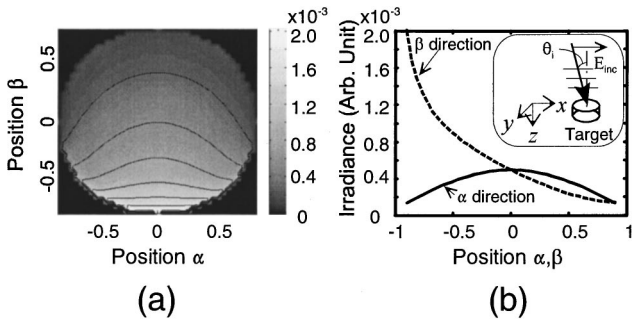

Fig. 7. Distribution of light diffracted by a small dielectric disk: (a) irradiance distribution, (b) cross section of (a). The diameter and the thickness of the disk are λ/2 and λ/50, respectively. The refractive index of the disk is 2.15. The incident light is linearly polarized, and the incident angle is 64° (s polarization).

We calculated diffraction patterns for oblique incident light to study the vectorial effect further. The incident light is linearly polarized in the xz plane. Incident angle θ_i is 64°, which corresponds to a NA of 0.9. We selected two incident directions with which to compare the diffraction patterns for p polarization and s polarization. Results are shown in Figs. 5–8. Figures 5 and 6 show the diffraction patterns for p-polarized light, where the incident light is in the xz plane. Figures 7 and 8 show the diffraction patterns for s-polarized light, where the incident light is in the yz plane. A small dielectric disk, λ/2 (325 nm) in diameter, is assumed as a target in Figs. 5 and 7, and a large dielectric disk, λ (650 nm) in diameter, is assumed as a target in Figs. 6 and 8. The diffraction patterns for p-polarized incident light (Figs. 5 and 6) show complex distribution patterns and larger dependence on target size than the patterns for s-polarized incident light (Figs. 7 and 8). This result implies that the z component of the electric field inside the target has a significant effect on the diffraction patterns. In addition, the vectorial effect on diffraction is greater for p-polarized light than for s-polarized light.

C. Electric Fields at the Target

When dipole polarizations P_j are obtained, the electric field at each point dipole can be calculated as

$$E_j = P_j/\alpha_j . \tag{9}$$

As an example, calculation results for normal incidence are shown in Figs. 9 and 10. These figures show the electric field distribution at the top surface of the dielectric disk of diameter λ/2 (325 nm), and the dielectric square plate of λ/2 × λ/2 (325 nm × 325 nm) sides, respectively. Only the electric field inside the target is shown in these figures, and the field outside is set at zero, although there is a nonzero field outside the target. In Fig. 10, a square area slightly larger than the square target is shown for each amplitude and phase distribution, so the distribution about the boundary can be clearly observed. The gray scale of each amplitude distribution is normalized by its peak value, as written below the distribution. Since the incident light is polarized in the x direction, the x component is dominant in the amplitude distributions. However, y and z components induced by the interaction of the fields inside the disk are not negligible and exhibit distinctive features in both amplitude and phase distributions.

The electric field distributions at the top of the large dielectric disk, λ (650 nm) in diameter, and the large dielectric square plates of λ × λ (650 nm × 650 nm) sides, are also calculated. The results are not shown in this paper, but the distributions have features similar to the corresponding distributions for the small disk in Fig. 9 and the small square plate in Fig. 10, respectively.

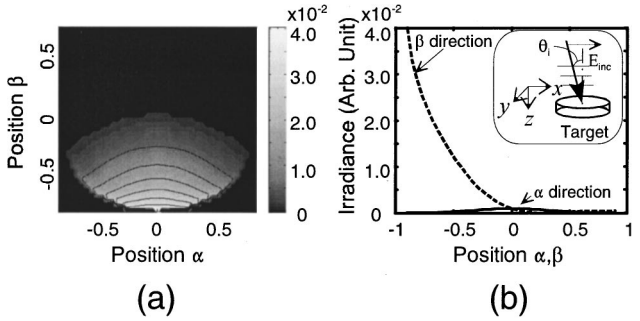

Fig. 8. Distribution of light diffracted by a large dielectric disk: (a) irradiance distribution, (b) cross section of (a). The diameter and the thickness of the disk are λ and λ/50, respectively. The refractive index of the disk is 2.15. The incident light is linearly polarized, and the incident angle is 64° (s polarization).

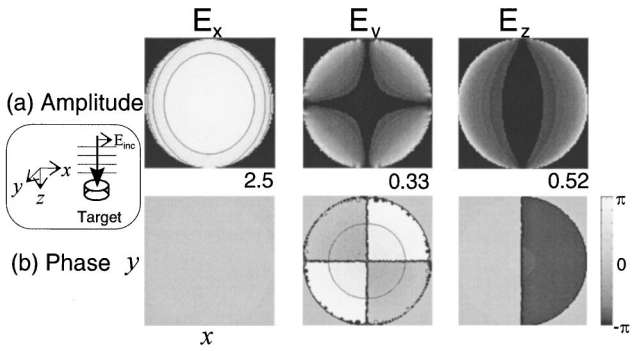

Fig. 9. Electric field distribution at a top surface of a small dielectric disk: (a) amplitude for x, y, and z components; (b) phase corresponding to (a). The diameter and the thickness of the disk are $\lambda/2$ and $\lambda/50$, respectively. The refractive index of the disk is 2.15. The incident light is linearly polarized, and the incident angle is 0°.

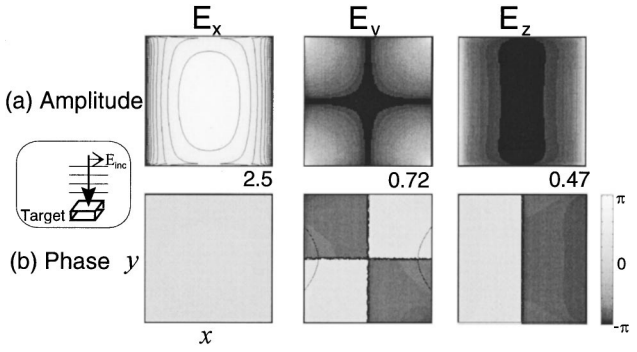

Fig. 10. Electric field distribution at a top surface of a small dielectric square plate: (a) amplitude for x, y, and z components, (b) phase corresponding to (a). The size of a side and the thickness of the square are $\lambda/2 \times \lambda/2$ and $\lambda/50$, respectively. The refractive index of the plate is 2.15. The incident light is linearly polarized, and the incident angle is 0°.

4. VALIDITY OF THE CALCULATIONS

Convergence and accuracy of the calculations are the important issues in this analysis. Draine and Flatau[2] and Piller[7] studied these issues for dielectric spheres in vacuum and showed that the calculations of scattering efficiency factors converge well and that accuracies of a few percent can be achieved. Similar results are expected for our calculations because we use the same method with the same criteria for validity: (1) $|n|kd \leqslant 1$ and (2) d must be small enough to describe the target shape satisfactorily. To evaluate convergence and the accuracy of our calculations, we analyzed the errors and the dependence of the distribution of the diffracted light on the spacing between the dipoles in one of our calculations.

First, the error in solving Eq. (6) for the small dielectric disk was analyzed. Since the equation is solved by the complex-conjugate gradient method, the error depends on the number of iterations in the method. The dependence of the error defined in expression (7) is shown in Fig. 11. The diameter and the thickness of the disk are $\lambda/2$ (325 nm) and $\lambda/50$ (13 nm), respectively. The spacing between the dipoles is $\lambda/197$ (3.3 nm). The refractive index of the disk is 2.15. The incident light is linearly polarized, and the incident angle is 0°. The wavelength of the light is 650 nm. These results show that the error is reduced quickly as the number of iterations increases. An error of less than 2×10^{-5} is achieved in seven iterations.

Next, the dependence of the distribution of the diffracted light on the number of iterations was investigated. The same target parameters were assumed. The distribution of the diffracted light calculated with P obtained in 13 iterations was used as a reference distribution, E_{ref}, and the error, defined by

$$e_{\mathrm{far}} \equiv \frac{\int\int |E_{\mathrm{far}} - E_{\mathrm{ref}}|^2 \mathrm{d}\alpha \mathrm{d}\beta}{\int\int |E_{\mathrm{ref}}|^2 \mathrm{d}\alpha \mathrm{d}\beta}, \tag{10}$$

was calculated. The result is shown in Fig. 12. The error in the distribution decreases quickly as the number of iterations increases and becomes sufficiently small in more than seven iterations.

Finally, we estimated dependence of the distribution of the diffracted light on the space d between the dipoles, assuming the same target parameters. The distribution of the diffracted light calculated with P obtained with $d = \lambda/406$ (1.6 nm) was used as a reference distribution E_{ref}, and the error defined by Eq. (10) was calculated. The result is shown in Fig. 13. The error in the distribution decreases quickly as d decreases, and it becomes less than 1% when $d = \lambda/197$ (3.3 nm).

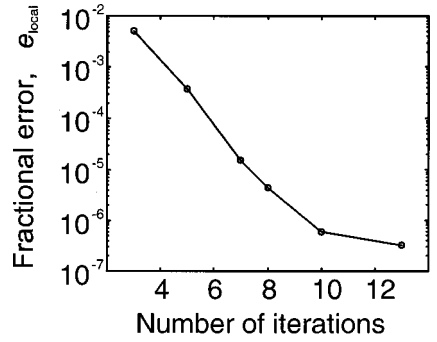

Fig. 11. Dependence of the error $e_{\mathrm{local}} \equiv |A \times P - E_{\mathrm{inc}}|/|E_{\mathrm{inc}}|$ on the number of iterations for a small dielectric disk. The diameter and the thickness of the disk are $\lambda/2$ and $\lambda/50$, respectively. The refractive index of the disk is 2.15. The incident light is linearly polarized, and the incident angle is 0°.

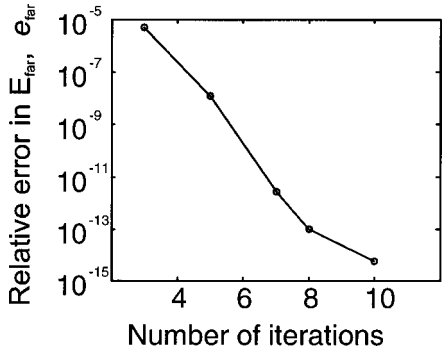

Fig. 12. Dependence of the error $e_{\mathrm{far}} \equiv \int\int |E_{\mathrm{far}} - E_{\mathrm{ref}}|^2 \mathrm{d}\alpha \mathrm{d}\beta / \int\int |E_{\mathrm{ref}}|^2 \mathrm{d}\alpha \mathrm{d}\beta$ on the number of iterations for a small dielectric disk. The distribution of the diffracted light calculated with P obtained by 13 iterations is used as E_{ref}. The diameter and the thickness of the disk are $\lambda/2$ and $\lambda/50$, respectively. The refractive index of the disk is 2.15. The incident light is linearly polarized, and the incident angle is 0°.

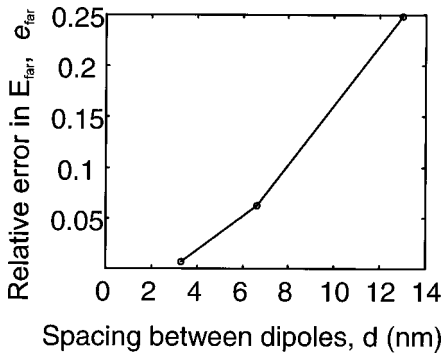

Fig. 13. Dependence of the error $e_{\mathrm{far}} \equiv \int\int |E_{\mathrm{far}} - E_{\mathrm{ref}}|^2 \mathrm{d}\alpha \mathrm{d}\beta / \int\int |E_{\mathrm{ref}}|^2 \mathrm{d}\alpha \mathrm{d}\beta$ on the spacing between dipoles d for a small dielectric disk. The distribution of the diffracted light calculated with P obtained with $d = 1.6$ nm ($\lambda/406$) is used as E_{ref}. The diameter and the thickness of the disk are $\lambda/2$ and $\lambda/50$, respectively. The refractive index of the disk is 2.15. The incident light is linearly polarized, and the incident angle is 0°.

These results in addition to previous analyses[2,7] support the validity of our calculations, although they may not guarantee it.

5. APPLICATION TO DIFFRACTION ANALYSIS FOR OPTICAL DATA STORAGE

Two major modifications have to be included in the analysis method described above if the method is to be applied to diffraction analysis in optical data storage systems. First, target structures have to be buried in other materials or on a surface in optical data storage systems, since marks on the recording medium are sandwiched between dielectric layers in many cases. Simple cases of dielectric targets buried in other materials may be handled by replacement of the dielectric constant of vacuum ϵ_0 in Eqs. (3) and (4) with the dielectric constant of the material surrounding the target. However, a detailed analysis should be performed to confirm this. We can calculate the diffraction from targets on a surface by applying the method developed by Taubenblatt and Tran.[8] Second, the method developed by Piller[7] has to be included so that materials with large refractive indices, such as metals and phase-change materials, can be used as target materials.

Vector diffraction analysis by the modified DDA can be applied to the diffraction analysis of optical data storage systems in the following way: Light incident upon the objective lens is focused onto the recording medium. The converging light is decomposed into a set of plane waves, and the polarization of each plane wave is described in terms of polarization components of the light incident upon the objective lens.[9–12] The distribution of diffracted light is calculated by the modified DDA.

6. CONCLUSIONS

The discrete-dipole approximation (DDA) method has been applied for vector diffraction analysis. The distributions of light diffracted by a subwavelength dielectric target in vacuum were analyzed, and the effect of the incident polarization was discussed. The electric field distributions inside the target were calculated, and their distinctive features were clearly presented. This technique facilitates understanding of the basic features of vector diffraction from small particles.

K. Shimura's e-mail address is shimura.kei@nifty.ne.jp; that of T. D. Milster is milster@arizona.edu.

REFERENCES

1. E. M. Purcell and C. R. Pennypacker, "Scattering and absorption of light by non-spherical dielectric grains," Astrophys. J. **186**, 705–714 (1973).
2. B. T. Draine and P. J. Flatau, "Discrete-dipole approximation for scattering calculations," J. Opt. Soc. Am. A **11**, 1491–1499 (1994).
3. T. Wriedt and U. Comberg, "Comparison of computational scattering methods," J. Quant. Spectrosc. Radiat. Transfer **60**, 411–423 (1998).
4. K. Shimura and T. D. Milster, "Analysis of three-dimensional distributions of scattered light by the discrete dipole approximation," in *Diffractive Optics and Micro-Optics*, 2000 OSA Technical Digest Series (Optical Society of America, Washington, D.C., 2000), pp. 162–164.
5. B. T. Draine and J. Goodman, "Beyond Clausius–Mossotti: wave propagation on a polarizable point lattice and the discrete dipole approximation," Astrophys. J. **405**, 685–697 (1993).
6. B. T. Draine and P. J. Flatau, "The discrete dipole approximation for scattering and absorption of light by irregular particles," http://www.astro.princeton.edu/~draine/DDSCAT.html.
7. N. B. Piller, "Coupled-dipole approximation for high permittivity materials," Opt. Commun. **160**, 10–14 (1999).
8. M. A. Taubenblatt and T. K. Tran, "Calculation of light scattering from particles and structures on a surface by the coupled-dipole method," J. Opt. Soc. Am. A **10**, 912–919 (1993).
9. M. Mansuripur, "Distribution of light at and near the focus of high-numerical-aperture objectives," J. Opt. Soc. Am. A **3**, 2086–2093 (1986).
10. M. Mansuripur, "Certain computational aspects of vector diffraction problems," J. Opt. Soc. Am. A **6**, 786–805 (1989).
11. M. Mansuripur, "Distribution of light at and near the focus of high-numerical-aperture objectives: erratum"; "Certain computational aspects of vector diffraction problems: erratum," J. Opt. Soc. Am. A **10**, 382–383 (1993).
12. D. G. Flagello, T. D. Milster, and A. E. Rosenbluth, "Theory of high-NA imaging in homogeneous thin films," J. Opt. Soc. Am. A **13**, 53–64 (1996).